Imaging Nanostructural Modifications Induced by Electronic Metal–Support Interaction Effects at Au||Cerium-Based Oxide Nanointerfaces

Miguel López-Haro,[†,∥] José M. Cíes,[†] Susana Trasobares,[†] José A. Pérez-Omil,[†] Juan J. Delgado,[†] Serafín Bernal,[†] Pascale Bayle-Guillemaud,[‡] Odile Stéphan,[§] Kenta Yoshida,[⊥] Edward D. Boyes,[⊥] Pratibha L. Gai,[⊥] and José J. Calvino[†,*]

[†]Departamento de Ciencia de los Materiales e Ingeniería Metalúrgica y Química Inorgánica, Facultad de Ciencias, Universidad de Cádiz, Campus Río San Pedro, E-11510 Puerto Real (Cádiz), Spain, [‡]CEA-INAC/UJF-Grenoble1 UMR-E, SP2M, LEMMA, Minatec Grenoble F-38054, France, [§]Laboratoire de Physique des Solides, UMR 850 University Paris Sud, 91405 Orsay, France, and [⊥]Departments of Chemistry and Physics, University of York, JEOL Nanocentre, Heslington, York YO10 5DD, United Kingdom. [∥]Present address: CEA-INAC/UJF-Grenoble1 UMR-E, SP2M, LEMMA, Minatec Grenoble, F-38054, France.

ABSTRACT

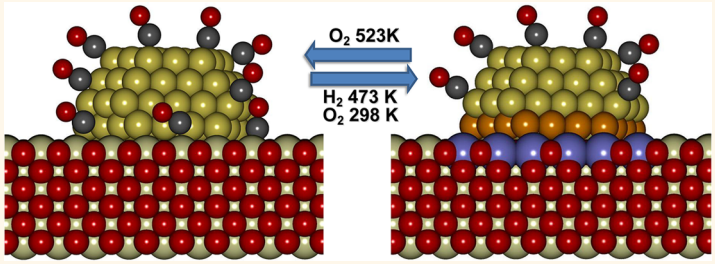

A variety of advanced (scanning) transmission electron microscopy experiments, carried out in aberration-corrected equipment, provide direct evidence about subtle structural changes taking place at nanometer-sized Au||ceria oxide interfaces, which agrees with the occurrence of charge transfer effects between the reduced support and supported gold nanoparticles suggested by macroscopic techniques. Tighter binding of the gold nanoparticles onto the ceria oxide support when this is reduced is revealed by the structural analysis. This structural modification is accompanied by parallel deactivation of the CO chemisorption capacity of the gold nanoparticles, which is interpreted in exact quantitative terms as due to deactivation of the gold atoms at the perimeter of the Au||cerium oxide interface.

KEYWORDS: gold catalysts · STEM · nanointerfaces · ceria · electronic metal–support interaction effects

Gold supported on ceria and closely related cerium-containing mixed oxide catalysts are known to constitute an interesting family of highly active materials for a variety of reactions.[1−11] Despite the very challenging problems to be overcome for their chemical and nanostructural characterization, in recent years, significant progress has been made in understanding the chemical principles governing the CO adsorption on them.[12−15] Thus, the contribution of both the metal phase and the oxide supports could be quantitatively determined for a series of powder ceria-zirconia-supported gold (Au/CZ) catalysts.[13,15] Likewise, it has recently been shown[12,14] that the CO adsorption capacity of a Au/CZ catalyst may be strongly inhibited by application of a rather mild reduction treatment at 473 K.[12,14] This deactivation was found to be reversible, with the normal behavior of the unreduced catalysts being fully recovered by further reoxidation of the prereduced catalyst at 523 K. As discussed in ref 12, these changes of chemical behavior are due to parallel modifications in the redox state of the support, and inherent to them, in the electronic interactions occurring between the metal nanoparticles and the support. In connection with these metal/support interaction effects, very recent DFT calculations carried out by Remediakis *et al.*[16] have suggested that, in the case of Au/TiO_2 catalysts, electron transfer from reduced titania to gold nanoparticles would mainly affect the metal atoms at the interface, that is, those in direct contact with the titania surface. Though similar calculations are not currently available for ceria-based gold catalysts, a parallel behavior could in principle be expected. If so, the nanostructure of the metal||oxide interfaces should be modified by the redox nature of the treatments applied to the catalysts. Moreover, the parallel modification of the chemical properties of gold should be particularly noticeable on the metal atoms in contact with the reduced support.

* Address correspondence jose.calvino@uca.es.

Received for review April 9, 2012 and accepted July 12, 2012.

Published online July 12, 2012
10.1021/nn301557u

This paper is aimed at exploring the two hypotheses of a ceria-based gold catalyst advanced above: the eventual occurrence of nanostructural changes at the metal/support interface and the concomitant modification of the adsorption capability of the gold atoms located at such an interface. To gain quantitative information about these two major goals, chemical data (volumetric adsorption of CO and oxygen storage capacity), high-resolution nanoanalytical (EELS), nanostructural, high-angle annular dark-field scanning transmission electron microscopy (HAADF-STEM), and high-resolution transmission electron microscopy (HRTEM) studies carried out on aberration-corrected (AC) microscopes are combined. By using aberration-corrected instruments, the spatial resolution required to unveil the very subtle structural modifications occurring in so highly localized regions of the catalyst could be achieved. The investigated catalyst consisted of a 1.5 wt % Au/$Ce_{0.5}Tb_{0.12}$ $Zr_{0.38}O_2$ (Au/CTZ) sample. Details of its preparation and characterization are given in the Experimental Section and references therein.

Due to their sensitivity to the atomic number,[17,18] AC-HAADF images are particularly well-suited to reveal the position of the heaviest elements at both sides of the metal/support interface: Au atoms on the nanoparticle side, and Ce, Tb, and Zr cations at the support side. Likewise, under appropriate and optimized recording conditions, AC microscopes may avoid the contrast delocalization effects[19] which very much complicate the structural analysis of interfaces in conventional, noncorrected, instruments. In this way, AC-HRTEM images may also be used to locate the positions of the interface atoms with high accuracy.

The onset of the metal−support interaction effect in the investigated Au/CTZ catalyst has been followed by monitoring the changes occurring in volumetric measurements of CO adsorption. The reduced state of the support has been investigated by means of oxygen storage capacity (OSC) measurements and electron energy loss spectroscopy. Finally, structure modeling has been used to interpret the CO chemisorption data, as proposed in ref 15.

The whole set of results not only illustrates the high potential of AC-(S)TEM to explore very fine nanostructural details of the Au/oxide interface, of extraordinary relevance in heterogeneous catalysis, but also, to the best of our knowledge, provides the first experimental evidence of the very subtle modifications in the metal/CTZ distance induced by the reduction of the support and inherent onset of electron transfer phenomena between the reduced support and the Au nanoparticles. Finally, an atomistic model has been used to interpret, in quantitative terms, the loss of CO chemisorption capacity of the metal in the prereduced Au/CTZ catalyst. The interpretation thus proposed fully confirms the predictions of DFT calculations.[16]

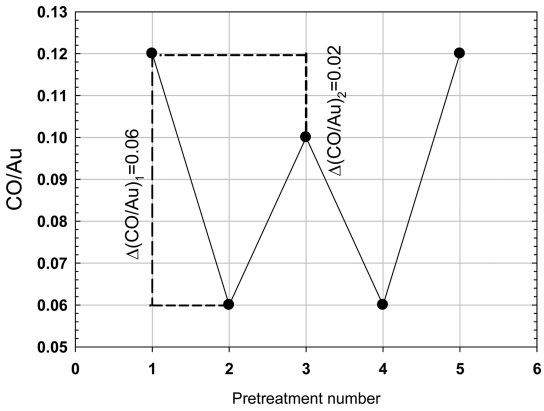

Figure 1. Values of the CO/Au ratios after the following consecutive pretreatments: (1) oxidation at 523 K; (2) pretreatment 1 followed by reduction at 473 K; (3) pretreatment 2 followed by reoxidation at 308 K; (4) pretreatment 3 followed by reduction at 473 K; (5) pretreatment 4 followed by oxidation at 523 K.

RESULTS AND DISCUSSION

Figure 1 shows the evolution of the CO/Au ratio values measured on the Au/CTZ catalyst after different pretreatments. To estimate these values, we have followed the approach described in ref 15 (details can be also found in Figure SI.1 and SI.2 of Supporting Information). These ratios express the fraction of the whole ensemble of gold atoms present in the catalyst which are capable of adsorbing CO. In the particular case of Au nanoparticles, it has been recently proven[15] that these atoms are not exactly all those exposed at the surface, as it indeed occurs for the interaction of CO with other noble metals such as Pt, but only those whose coordination numbers are not higher than 7 (*i.e.*, only a fraction of the total surface atoms). Thus, in the preoxidized catalyst, the CO/Au ratio is 0.12. This value corresponds very closely to the total number of gold atoms on the surface of the nanoparticles with a coordination number ≤ 7 (0.14, Table SI.1 Supporting Information). When the preoxidized catalyst is further reduced at 473 K, the CO/Au ratio decreases to 0.06, that is, to 50% of the original value. Reoxidation of the reduced catalyst at room temperature (308 K) partially recovers the adsorption capacity of the metal, to 83% of the original value, with the CO/Au ratio increasing back to 0.10. An additional reduction treatment at 473 K reproduces the effect of the previous reduction, leading again to a CO/Au ratio equal to 0.06. In good agreement with the results reported in ref 12 to fully recover the catalyst from the deactivated state resulting from the reduction at 473 K, it must be reoxidized at 523 K; after which, the highest CO/Au ratio, 0.12, was measured again.

This behavior is exactly parallel to that recently reported for a Au/ceria-zirconia catalyst.[14,15] As revealed by volumetric studies of oxygen adsorption at 523 K (Figure SI.3 in Supporting Information), the OSC determined for the Au/CTZ catalyst prereduced at 473 K is equivalent to 37% reoxidation of the CTZ support. When the oxygen

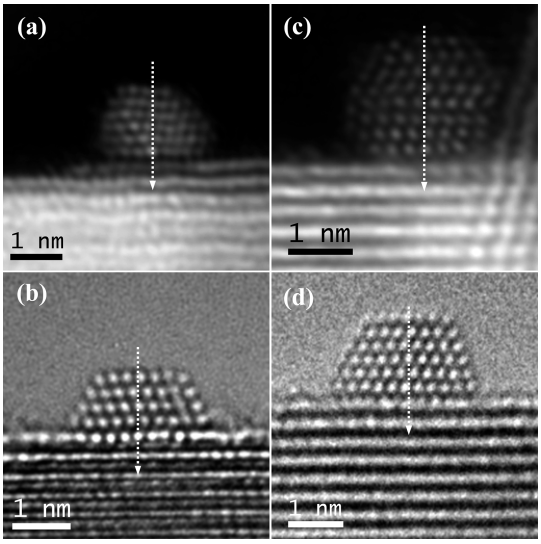

Figure 2. Experimental images of the Au (1.5 wt %)/ $Ce_{0.5}Tb_{0.12}$ $Zr_{0.38}O_2$ catalyst, after reduction at 473 K and further reoxidation at 308 K ((a) AC-HAADF image, (b) AC-HRTEM image); after oxidation at 523 K ((c) AC-HAADF image, (d) AC-HRTEM image).

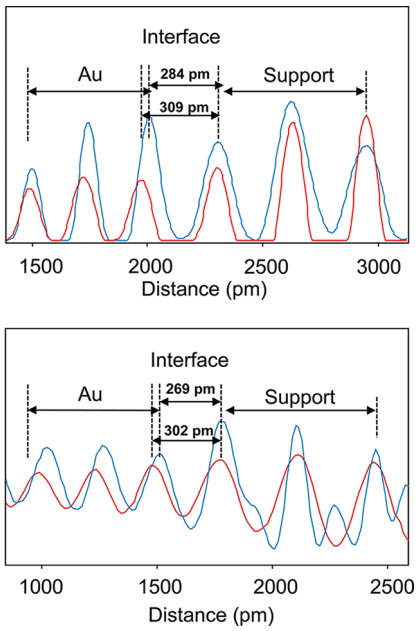

Figure 3. (Top) Superposition of the intensity profiles recorded from the AC-HAADF images of the oxidized catalyst (red trace) and the reduced and reoxidized catalyst (blue trace); (bottom) same but starting from the AC-HRTEM images. In both plots, the maxima corresponding to the oxide support have been aligned.

adsorption is measured at room temperature, 308 K, the corresponding OSC value for the catalyst reduced at 473 K was found to be 23%, thus indicating that, at 308 K, 14% of the reduced CTZ support is not reoxidized.

These results demonstrate that the CO adsorption capacity of the metal nanoparticles in the Au/CTZ catalyst is largely influenced by the redox state of the underlying support.

Figure 2 shows representative AC-HAADF and AC-HRTEM images of the Au/CTZ sample after the initial oxidation treatment (right column) and after further reduction at 473 K and reoxidation at room temperature (left column). In the case of AC-HAADF images, the column ratio mapping processing technique[20] was applied to improve the accuracy of the quantitative analysis. Note that the gold nanoparticles are easily observed on the surface of the CTZ support. In both types of images, the white contrasts locate the position of the heavy elements, the gold atoms on the nanoparticle side of the interface, and the metal cations on the support side. In the case of AC-HAADF, the intensity in the images is related to roughly the value of Z^2. The AC-HRTEM images were acquired to image atomic columns as white contrasts, with a defocus value close to zero.[21]

A first analysis of the structural parameters of the Au||CTZ interfaces was performed by taking intensity line profiles along paths normal to the interface, starting at the metal particle, crossing the interface region, and ending in the bulk of the support crystallites, as marked with dashed white lines on the experimental images. The resulting profiles are shown in Figure 3. Each peak in these profiles corresponds to one lattice plane, so the distance between maxima provides a measurement of distances between adjacent planes.

Akita *et al.*[22,23] have used this approach with conventional, noncorrected, HAADF and HRTEM images to compare the interfaces of Au/TiO_2 and Au/CeO_2 catalysts. However, in these papers, the influence of the oxidation state of the supports, which is the central point of our contribution, is not considered.

Taking into account the magnification at which the images were recorded and the 2k $\times$ 2k size of the digital images, the pixel size of these measurements was 6 pm for AC-HAADF images and 10 pm for AC-HRTEM images. For subpixel resolution, improving the quality of distance measurements beyond the values reported above, all intensity profiles were fitted to sets of Gaussian functions. Distance measurements were then obtained from differences between the corresponding optimized maxima values resulting from fitting.

The profiles corresponding to the oxidized catalyst (red traces), which will be referred to hereafter as AuCTZ-Ox, are superimposed to that of the reduced and room temperature reoxidized ones (blue traces) (AuCTZ-Red) in the two plots of Figure 3. The traces of the two pretreatments have been aligned to each other using the maxima of the ceria-terbia-zirconia support, at the right side of the plots, so as to allow an easier comparison between them. The differences in the {111} interplanar distances of the support attributable to differences in their reduction state (Ln^{3+} content) lie in the range of 2−3 pm, which is below our pixel resolution. Therefore, the alignment of the two profiles in the support region is reasonable.

There is a first qualitative aspect of these profiles worth highlighting, the shift of the Au{111} peaks

between the oxidized and the reduced catalysts. Note particularly that this shift, which is visible in the comparison of both the AC-HAADF and AC-HRTEM profiles, starts just at the metal−support interface; that is, it is first established between the last {111} peak of the support and the first {111} of the Au nanoparticle. Thus, if we focus on the profiles obtained from the AC-HAADF images, a first estimate of the Au-to-support interface distance reveals values of 284 and 309 pm for the AuCTZ-Ox and AuCTZ-Red catalysts, respectively. Therefore, according to the profiles obtained from AC-HAADF, the difference between these distances is about 25 pm. Similarly, different interface distance values can be estimated from the profiles of the AC-HRTEM images: 269 and 302 pm for the oxidized and reduced catalyst, respectively. The difference in this case amounts to 28 pm.

The agreement found in the trends of the measurements observed by these two so different techniques provides initial support for the validity of the estimations performed. Nevertheless, to get an assessment of the accuracy of these interface distance measurements, which are influenced by experimental image recording parameters such as drift or scan noise among others, an error estimation was performed by analyzing in detail a number of intensity profiles recorded on both the reduced and the oxidized catalysts. Using the collection of Gaussian-fitted profiles, the distance between adjacent {111} support and {111} Au peaks was measured with subpixel resolution. In the case of the interfaces, several profiles were obtained at different positions to improve statistics. Figure 4 plots the results of this analysis carried out separately on both types of images, AC-HAADF and AC-HRTEM. Average values with their corresponding error bars are shown for distances between the support planes, between the metal planes, and between Au and support.

Note how, independently of the imaging technique used, the Au{111} distances measured on the oxidized and the reduced catalysts are indistinguishable, with the ranges observed in the experimental measurements overlapping to a large extent in both cases. The same observation is also valid for the CTZ−support {111} distances. In other words, average values of Au{111} and CTZ−support {111} are very close in both catalysts and in any case within the range of experimental errors. In contrast, the average values measured for the Au-to-support distances at the interface on the oxidized and reduced catalysts are neatly separated, with overlapping of the corresponding error bar ranges not being observed.

Thus, whereas the difference between Au{111} average values of the oxidized and reduced catalysts amounts to only 5 pm (ex HAADF) or 2 pm (ex HRTEM) and the difference between CTZ−support {111} amounts to just 2 pm (ex HAADF) or 3 pm (ex HRTEM), these differences increase up to 25 pm (ex HAADF) or 31 pm (ex HRTEM) in the case of the Au/CTZ−support interface distance.

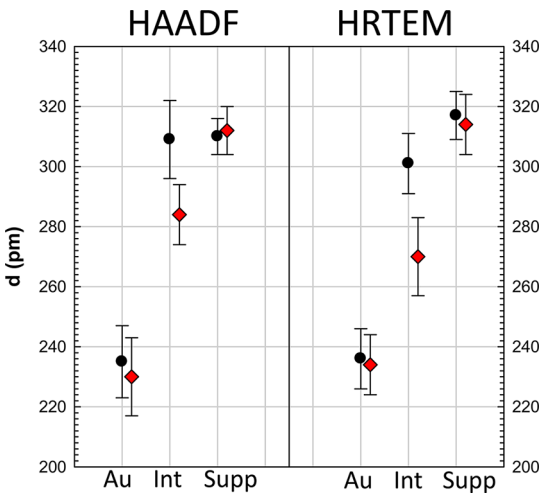

Figure 4. Average values of Au{111}, CTZ−support {111}, and Au−support distances determined from the complete analysis of a few intensity profiles. Left side plots the results obtained from the analysis of AC-HAADF images, and right side those of profiles recorded from AC-HRTEM ones. Error bars are marked for each measurement. Dots: AuCTZ-Ox catalysts. Diamonds: AuCTZ-Red catalyst.

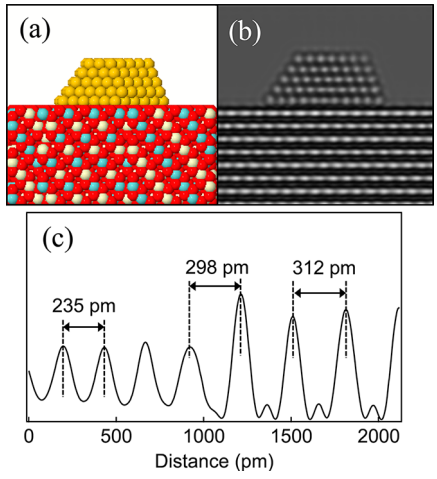

Figure 5. (a) Structural model of a Au/$Ce_{0.5}Tb_{0.12}Zr_{0.38}$ catalyst to interpret the AC-HRTEM image of Figure 2d and which considers a Au-to-support distance of 298 pm. (b) Simulated AC-HRTEM for $\Delta f = -10$ nm. (c) Intensity profile along the normal to the interface. Relevant distances are marked.

To estimate how close the distances measured on the experimental images corresponded to the actual distance between the planes at the interface, image simulation studies were performed which have allowed us to evaluate the influence of another imaging parameter, defocus. Figure 5 shows the results corresponding to the simulation of AC-HRTEM images. In this case, a model comprising a gold nanoparticle on a $Ce_{0.5}Tb_{0.12}Zr_{0.38}O_2$ support was built (Figure 5a). The model was considered to specifically gave a Au-to-support distance of 298 pm, which is in fact the average interface distance for the AuCTZ-Ox catalyst (see further). In the corresponding simulated image (Figure 5b), both the gold atoms and the cation columns in the support are

imaged, as previously mentioned, in the form of white contrasts. The distances which can be measured on the intensity profile obtained from this simulation (Figure 5c) correspond very closely to those in the model: 312 pm for the {111} planes of the CTZ−support, 235 pm for the {111} planes of Au, and 298 pm for the interface distance between the metal particle and support. A similar analysis on images simulated for other defocus values in the range of the experimental one (Figure SI.4 of Supporting Information) reveals differences in the order of just 4 pm with respect to the nominal value. This clearly proves that the distances measured on the profiles of experimental AC-HRTEM images can be interpreted as those present in the material as well as a reasonable stability of the interface distance measurements with respect to the experimental recording parameter of defocus.

Once the measurements were proven to be reasonably reliable, that is, that they reproduced the actual distances existing in the specimen within the required accuracy, to obtain statistically meaningful values for the parameter which has been determined, the distance between metal and support planes at the interface, a large number of AC images, both HAADF and HRTEM, were analyzed. This last analysis would bring into consideration the influence of other possible imaging and sample parameters like mistilt of the imaged interface with respect to the incoming electron beam or metal particle size, among others. The whole ensemble of measurements can then be statistically analyzed, as shown in Figure 6, which plots the distribution of this parameter for the two catalysts. In both cases, measurements lie within a certain range, but note how in the AuCTZ-Ox catalyst there is a clearly higher contribution of measurements corresponding to larger distances. In fact, the average values obtained for these two distributions are 298 pm for AuCTZ-Ox and 285 pm for AuCTZ-Red. As also shown in Figure 6, 85% of the measurements made on AuCTZ-Ox are larger than the average value of the AuCTZ-Red catalyst. Likewise, 77% of the measurements made on the latter are smaller than the average value of AuCTZ-Ox.

All of these figures clearly indicate that there is a statistically significant difference between the two catalysts concerning the distance between the planes of the metal and the support in contact at the interface. This distance is about 13 pm shorter in the catalyst that has been reduced at 473 K and reoxidized at room temperature.

The small difference in the pretreatments between the two catalysts, thermal treatments at very low temperatures (not higher than 473 K), allows initially disregarding possible changes in the cationic composition of the oxide surface as responsible for the changes detected at the interface. Thus, according to a number of previous studies,[24−27] the mobilization of the cationic sublattice in ceria-zirconia mixed oxides takes place under reducing conditions at temperatures around 1173 K and at temperatures above 1073 K under

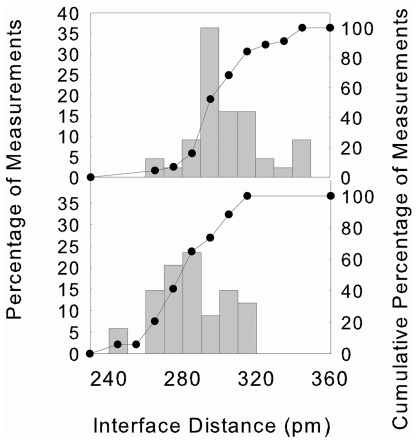

Figure 6. Distributions of the Au-to-support distances at the interface for the two catalysts: (top) oxidized at 523 K; (bottom) reduced at 473 K and reoxidized at 308 K. The black dot plots correspond to the cumulative number of measurements.

oxidizing environments. These temperature thresholds are far greater than those used to go from the AuCTZ-Ox to the AuCTZ-Red catalysts studied here. Therefore, the interface differences must stem from other alternative structural effects. Differences in the reduction state of the support seems to be the appropriate candidate.

Thus, we have to recall (Figure SI.3 in Supporting Information) that the AuCTZ-Red catalyst contained at least 14% of lanthanide species in reduced state (*i.e.*, as Ln^{3+}). If we take into account that changing from the +4 oxidation state to the +3 involves an increase of the cationic radius,[28] about +10 pm in the case of changing from Ce^{4+} to Ce^{3+}, and +16 pm in the case of moving from Tb^{4+} to Tb^{3+}, the expected result for a nanoparticle that it is not affected by the reduction effects in the support would be increasing the distance to gold by about +11 pm (average value weighted by Ce/Tb composition). We observe just the opposite, hence our data show that the nanoparticle is getting closer to the surface of the reduced ceria-terbia-zirconia support. From our estimates of the changes in the average interface distance, the nanoparticles get about 24 pm closer to the surface. This can be interpreted as due to a tighter binding of the gold nanoparticles by the reduced support, as would be expected after an electron transfer from the reduced support to the gold nanoparticle.

OSC measurements reported previously clearly indicated that the AuCTZ-Red catalyst is not fully oxidized. One aspect we tried to clarify was the spatial distribution of the reduced lanthanide species. We have used electron energy loss spectroscopy (EELS) in scanning transmission electron microscopy mode (STEM) to study this aspect. In particular, a series of EEL spectra were recorded over time using a tiny electron probe on selected positions of the different catalysts. Two types of sites were monitored: (1) sites of the support containing a metal nanoparticle; (2) sites of the support far from metal particles. The chrono-spectroscopy mode,

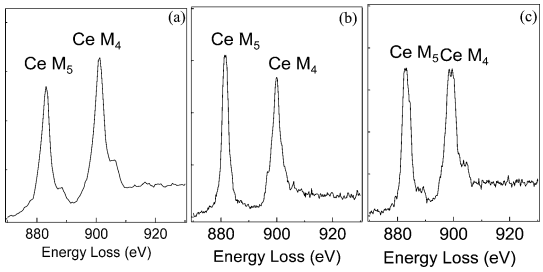

Figure 7. Representative EEL spectra recorded on (a) AuCTZ-Ox catalyst at sites at the metal−support interface, (b) AuCTZ-Red catalyst at sites at the metal−support interface, (c) AuCTZ-Red catalyst at sites at the surface of the support in the neighborhood of the metal particles.

acquiring spectra every 100 ms, allowed us to monitor in time the evolution of the oxidation state of the sample at the locations under analysis, this providing us with a tool to estimate the beam influence on our studies (Figure SI.5 in Supporting Information). Within the available range of experimental parameters, recording conditions were always selected that minimized the rate of oxidation state modification. Moreover, fresh areas of the catalysts, not submitted to previous irradiation, were selected for the analysis of the different locations. The spectra we report here correspond to recording times smaller than those we could establish as giving rise to the first noticeable oxidation state change effects. Total electron dose of the reported spectra was always on the order of 10^7 e^-/nm^2.

Concerning the possible influence of other beam damage mechanisms, like knock-on, oxygen seems to be the most sensitive candidate. According to the information in ref 29, the values of maximum transferable energy at accelerating voltages of either 80 or 200 kV are much lower than the 65 eV value reported in ref 30 for the threshold displacement energy (E_t) of O in ceramic oxides very close in composition and structure to the oxides we have studied here. Even assuming that the E_t value for positions at the interface would be lower than the bulk one, it seems reasonable to expect that the influence of knock-on is only very moderate.

Figure 7 depicts the results of the EELS study, in the energy range corresponding to Ce-$M_{4,5}$. For this element, it is well-known[31] that changes in the fine structure of the white lines can be correlated with the oxidation state of cerium. The exact position in energy of the M_4 and M_5 white lines, the relative intensity ratio of these lines, and the appearance of shoulders at the right side of the peaks in the case of Ce^{4+} can be used as the fingerprint of each oxidation state.[31] In the case of the AuCTZ-Ox catalyst, at sites lying at the gold nanoparticle||support interface, the features of the EEL spectra indicate that cerium is present mostly as Ce^{4+}. The same result is observed when the analysis comes from sites far away from the metal nanoparticles.

In contrast, when the analysis is performed on the AuCTZ-Red catalyst, the following is observed: (1) at sites where metal nanoparticles are located (Figure 7b), both

TABLE 1. Estimation of Ce^{3+} Contents at Specific Sites of the Two Au/CTZ Catalysts As Determined from Quantitative NNLS Analysis of EELS Spectra

catalyst	% Ce^{3+} at Sites 1	% Ce^{3+} at Sites 2
AuCTZ-Ox	12	9
AuCTZ-Red	62	26

Ce^{3+} and Ce^{4+} are present in significant quantities but the Ce^{3+} signal is dominant; (2) at surface sites off the metal nanoparticles (Figure 7c), a mixture of Ce^{3+} and Ce^{4+} with a larger content of the oxidized specie is present.

These qualitative conclusions have been further confirmed by the quantitative analysis of these EEL spectra performed by means of nonnegative least square (NNLS) fitting.[32,33] The percentage of Ce^{3+} species present in each catalyst and site type are gathered in Table 1. In the AuCTZ-Ox catalyst, although EELS data indicate that there is still the presence of a small fraction of Ce^{3+} species, most likely due to unavoidable reduction effects even at initial stages of exposure to the electron beam, the two types of sites showed similar contents of reduced species (Ce^{3+}). On the contrary, in the AuCTZ-Red catalyst, cerium is largely in the form of reduced Ce^{3+} species in the regions underlying the metal nanoparticles. Moreover, the amount of Ce^{3+} species at these sites is much larger than just outside the interface. That is, the remaining reduction after reoxidation at room temperature concentrates to some extent under the metal nanoparticles.

Summarizing the whole set of chemical and atomic scale characterization results presented up to now shows that after reduction at 473 K the Au/CTZ catalyst loses its CO chemisorption capacity. This is associated with a redox state of the support characterized by an OSC value of 37%. It becomes much lower, 14%, upon reoxidation at room temperature. In parallel with this change in the redox state of the support, the CO adsorption capacity of the gold nanoparticles is partly recovered, from a CO/Au value of 0.06 for the catalyst reduced at 473 K to CO/Au = 0.10 for the sample further reoxidized at 308 K, and to a still larger CO/Au value of 0.12 upon reoxidation at 523 K. From the structural point of view, it is clear that in the catalyst with 14% reduction of the support the gold nanoparticles are more tightly bonded to the support, as is reflected by the 24 pm (closer) approach between the atomic planes of gold and support at the interface evidenced by the analysis of the AC images. This interaction could be linked to an electron transfer between the reduced support lying just below the metal||support interface, as indicated in the analysis of cerium oxidation states performed by EELS and the metal nanoparticles. We should recall at this point that the occurrence of this electron transfer effect is supported by previous XPS and FTIR results of adsorbed CO described in detail in ref 12.

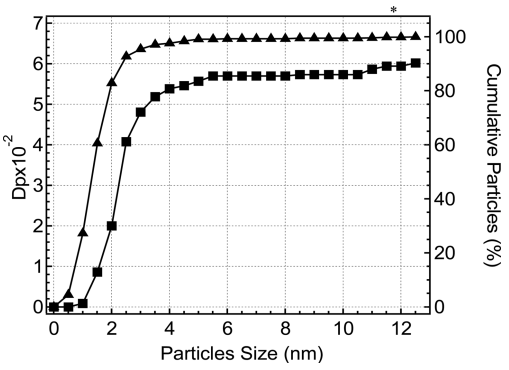

Figure 8. Cumulative plots with particle size: (square symbols) fraction of Au atoms at the perimeter of the interface plane between the metal nanoparticles and the support; (triangle) number of particles. AuCTZ-Red catalyst.

A final relevant question we have addressed is relating the quantitative values of the CO chemisorption inhibition detected in the two reduced catalysts, Δ(CO/Au), and the structure of their nanoparticle systems. As described previously, after reduction at 473 K, the CO/Au ratio decreases by $\Delta(CO/Au)_1 = 0.06$. The analysis of the distribution of coordination numbers of the gold atoms on the surface of the nanoparticles of the catalyst reduced at 473 K can be done from the particle size distribution and using the methodology reported in ref 15. Table SI.1 in Supporting Information indicates that the fraction of gold atoms at the perimeter of the contact planes between the metal nanoparticles and the support (D_p) is 0.06. This is the value reported for the decrease in the CO/Au ratio, $\Delta(CO/Au)_1$, indicating that the CO inhibition could be exactly assigned to the deactivation of the gold atoms at the perimeter of the interface plane. This is in very good agreement with the predictions made by Remediakis *et al.*[16] on the basis of DFT calculations.

Figure 8 plots the evolution with particle size of the cumulative fraction of gold atoms at the perimeter of the interface plane between the metal nanoparticles and the support (square symbols) in the Au/CTZ catalyst reduced at 473 K. The evolution of the total number of particles (triangle symbols) is also included. Note that to reach the value of 0.06, that is, the extent of the CO/Au ratio decrease after reduction, $\Delta(CO/Au)_1$, 100% of the particles should be considered. Given that reoxidation at room temperature does not change the particle size distribution at all, the same curves can be used for the Au/CTZ catalysts reduced at 473 K and further reoxidized at room temperature (*i.e.*, AuCTZ-Red). This being so, to account for the 0.02 decrease in the CO/Au ratio determined for this catalyst, $\Delta(CO/Au)_2$, the atoms at the perimeter of nanoparticles smaller or equal to 2 nm should be considered. These represent about 80% of the whole set of nanoparticles present in this catalyst. This would be a possible way to interpret this $\Delta(CO/Au)_2$ figure.

CONCLUSION

In summary, our results support, in exact quantitative terms, the fact that the deactivation of the CO chemisorption capacity might be due to the perturbation of the chemical properties of just the gold atoms at the metal||reduced−support interface as suggested by DFT calculations. The only atoms of these interfaces capable of chemisorbing CO are those at the perimeter of the interface, and there is an exact correlation between D_p and Δ(CO/Au). The perturbation of the chemical properties detected after reduction at 473 K is paralleled by a structural modification at the level of the interface reflected as an approach of the nanoparticles to the surface of the support in the reduced catalyst. This reflects a tighter binding of the gold nanoparticles on the reduced support. This structural modification, which also agrees well with previous XPS and FTIR data supporting the occurrence of changes in the electronic state of gold, should influence the catalytic performance of the system. Recently, Yates *et al.*[34] have evidenced the key role of Ti−Au dual sites at the perimeter of nanometer-sized nanoparticles in the CO oxidation reaction. Our OSC data show that full reoxidation of the support is only attained above room temperature. Thus, even under the oxidizing conditions typical of the CO/O_2 mixtures used to run CO oxidation assays, the catalyst could be working in the electronically perturbed state. Likewise, in other reactions working under net reducing environments, as is the case of water gas shift (WGS),[3,4,6,10] selective oxidation of CO in the presence of a large excess of H_2 (PROX),[2,5,8,11] or selective hydrogenation reactions,[7] the modifications at the perimeter sites induced by the redox state of the support could prevail over a wider range of temperatures.

Finally, we should highlight the high potential of aberration-corrected microscopy to investigate in detail the structural properties of interfaces whose dimensions do not exceed just a few nanometers, a very relevant feature for the very wide family of supported catalysts. As demonstrated in this contribution, these techniques are unique and provide information, out of reach for other characterization techniques, key to understanding in quantitative terms the behavior of these systems.

EXPERIMENTAL SECTION

The Au(1.5 wt %)/$Ce_{0.5}Tb_{0.12}Zr_{0.38}O_2$ (Au/CTZ) catalyst, with a BET surface area of 16 m^2g^{-1}, was prepared by deposition−precipitation methods starting from a commercial CTZ mixed oxide support kindly donated by Grace Davison. The gold precursor was 99.99% $H[AuCl_4]$, from Alfa Aesar. An aqueous solution of urea was used as precipitating agent. Further details about the preparation procedure are reported in ref 35. The metal loading was confirmed by ICP analysis.

Ultra-high-resolution high-angle annular dark-field scanning transmission electron microscopy images were recorded on the FEI Titan 80-300 microscope equipped with a probe Cs

corrector, operating at 300 kV at CEA Grenoble. A condenser aperture of 50 μm and a 128 mm camera length allowed us to obtain an electron probe with a convergence angle of 20 mrad. The aberrations of the condenser lenses were corrected up to third-order using the Zemlin tableau to obtain a sub-angstrom electron probe.

High-resolution transmission electron microscopy images were recorded in the JEOL2200FS double aberration-corrected transmission electron microscope, operating at 200 kV installed at the University of York-JEOL Nanocenter.[36] Only the objective lens corrector was used, and in the Zemlin tableau, the defocus and the third aberration coefficients of the objective lens were measured and adequately compensated for.

EELS spectra were recorded in the VG-HB501 dedicated STEM at Orsay, working at 80 kV and using a 15 mrad convergence semiangle and 24 mrad collection angle. The analysis was always performed on thin areas to avoid any contribution of plural scattering. The chrono-spectrum mode was used: this approach consists of acquiring a series of EELS spectra recorded over time using a 1 nm electron probe with 0.2 eV energy dispersion. The above-mentioned instrument allows the recording of electron energy loss spectra, with high signal-to-noise ratios, using acquisition times as small as 100 ms on the M4,5 Ce edge. This small total acquisition time avoids sample drift, which could eventually limit the spatial resolution of the measurements. At the same time, sample irradiation problems are also minimized under these conditions, thereby increasing the reliability of the analytical data.

The Au/ceria-zirconia-terbia catalyst models used in our HRTEM image simulation studies were built with RHODIUS, a computer program developed at our laboratory.[37] TEMSIM software was used for AC-HRTEM image simulations.[38]

Conflict of Interest: The authors declare no competing financial interest.

Acknowledgment. Financial support from the Ministry of Science and Innovation of Spain/FEDER Program of the EU (Projects MAT2008-00889-NAN, and CSD2009-00013) and the Junta de Andalucía (Groups FQM-110 and FQM-334) is acknowledged. The ceria-terbia-zirconia sample was kindly donated by Grace Davison Company. M.L.H. thanks the MECD Spanish Ministry (ref EX2010-1135) for funding his postdoctoral stay at CEA-Grenoble. J.M.C. thanks the University of Cádiz for support through a postdoctoral short-stage grant.

Supporting Information Available: Additonal experimental details. This material is available free of charge *via* the Internet at http://pubs.acs.org.

REFERENCES AND NOTES

1. Carrettin, S.; Concepcion, P.; Corma, A.; Nieto, J. M. L.; Puntes, V. F. Nanocrystalline CeO_2 Increases the Activity of an for CO Oxidation by Two Orders of Magnitude. *Angew. Chem., Int. Ed.* **2004**, *43*, 2538–2540.
2. Trimm, D. L. Minimisation of Carbon Monoxide in a Hydrogen Stream for Fuel Cell Application. *Appl. Catal., A* **2005**, *296*, 1–11.
3. Burch, R. Gold Catalysts for Pure Hydrogen Production in the Water-Gas Shift Reaction: Activity, Structure and Reaction Mechanism. *Phys. Chem. Chem. Phys.* **2006**, *8*, 5483–5500.
4. Deng, W. L.; Flytzani-Stephanopoulos, M. On the Issue of the Deactivation of Au-Ceria and Pt-Ceria Water-Gas Shift Catalysts in Practical Fuel-Cell Applications. *Angew. Chem., Int. Ed.* **2006**, *45*, 2285–2289.
5. Avgouropoulos, G.; Manzoli, M.; Boccuzzi, F.; Tabakova, T.; Papavasiliou, J.; Ioannides, T.; Idakiev, V. Catalytic Performance and Characterization of Au/Doped-Ceria Catalysts for the Preferential CO Oxidation Reaction. *J. Catal.* **2008**, *256*, 237–247.
6. Abd El-Moemen, A.; Karpenko, A.; Denkwitz, Y.; Behm, R. J. Activity, Stability and Deactivation Behavior of Au/CeO_2 Catalysts in the Water Gas Shift Reaction at Increased Reaction Temperature (300 °C). *J. Power Sources* **2009**, *190*, 64e75.
7. Cardenas-Lizana, F.; Gomez-Quero, S.; Perret, N.; Keane, M. A. Support Effects in the Selective Gas Phase Hydrogenation of *p*-Chloronitrobenzene over Gold. *Gold Bull.* **2009**, *42*, 124–132.
8. Chiorino, A.; Manzoli, M.; Menegazzo, F.; Signoretto, M.; Vindigni, F.; Pinna, F.; Boccuzzi, F. New Insight on the Nature of Catalytically Active Gold Sites: Quantitative CO Chemisorption Data and Analysis of FTIR Spectra of Adsorbed CO and of Isotopic Mixtures. *J. Catal.* **2009**, *262*, 169–176.
9. Huang, X.-S.; Sun, H.; Wang, L.-C.; Liu, Y.-M.; Fan, K.-N.; Cao, Y. Morphology Effects of Nanoscale Ceria on the Activity of Au/CeO_2 Catalysts for Low-Temperature CO Oxidation. *Appl. Catal., B* **2009**, *90*, 224–232.
10. Daly, H.; Goguet, A.; Hardacre, C.; Meunier, F. C.; Pilasombat, R.; Thompsett, D. The Effect of Reaction Conditions on the Stability of $Au/CeZrO_4$ Catalysts in the Low-Temperature Water-Gas Shift Reaction. *J. Catal.* **2010**, *273*, 257–265.
11. Tabakova, T.; Manzoli, M.; Vindigni, F.; Idakiev, V.; Boccuzzi, F. CO-Free Hydrogen Production for Fuel Cell Applications over Au/CeO_2 Catalysts: FTIR Insight into the Role of Dopant. *J. Phys. Chem. A* **2010**, *114*, 3909–3915.
12. Cies, J. M.; del Rio, E.; Lopez-Haro, M.; Delgado, J. J.; Blanco, G.; Collins, S.; Calvino, J. J.; Bernal, S. Fully Reversible Metal Deactivation Effects in Gold/Ceria-Zirconia Catalysts: Role of the Redox State of the Support. *Angew. Chem., Int. Ed.* **2010**, *49*, 9744–9748.
13. Cies, J. M.; Delgado, J. J.; Lopez-Haro, M.; Pilasombat, R.; Perez-Omil, J. A.; Trasobares, S.; Bernal, S.; Calvino, J. J. Contributions of Electron Microscopy to Understanding CO Adsorption on Powder Au/Ceria-Zirconia Catalysts. *Chem.—Eur. J.* **2010**, *16*, 9536–9543.
14. Delgado, J. J.; Cies, J. M.; Lopez-Haro, M.; del Rio, E.; Calvino, J. J.; Bernal, S. Recent Progress in Chemical Characterization of Supported Gold Catalysts: CO Adsorption on Au/Ceria-Zirconia. *Chem. Lett.* **2011**, *40*, 1210–1216.
15. Lopez-Haro, M.; Delgado, J. J.; Cies, J. M.; del Rio, E.; Bernal, S.; Burch, R.; Cauqui, M. A.; Trasobares, S.; Perez-Omil, J. A.; Bayle-Guillemaud, P.; *et al.* Bridging the Gap between CO Adsorption Studies on Gold Model Surfaces and Supported Nanoparticles. *Angew. Chem., Int. Ed.* **2010**, *49*, 1981–1985.
16. Remediakis, I. N.; Lopez, N.; Norskov, J. K. CO Oxidation on Gold Nanoparticles: Theoretical Studies. *Appl. Catal., A* **2005**, *291*, 13–20.
17. Pennycook, S. J.; Jesson, D. E. High-Resolution Incoherent Imaging of Crystals. *Phys. Rev. Lett.* **1990**, *64*, 938–941.
18. Pennycook, S. J.; Jesson, D. E. High-Resolution Z-Contrast Imaging of Crystals. *Ultramicroscopy* **1991**, *37*, 14–38.
19. Zandbergen, H. W.; Tang, D.; VanDyck, D. Non-linear Interference in Relation to Strong Delocalisation. *Ultramicroscopy* **1996**, *64*, 185–198.
20. Robb, P. D.; Craven, A. J. Column Ratio Mapping: A Processing Technique for Atomic Resolution High-Angle Annular Dark-Field (HAADF) Images. *Ultramicroscopy* **2008**, *109*, 61–69.
21. Yoshida, K.; Kawai, T.; Nambara, T.; Tanemura, S.; Saitoh, K.; Tanaka, N. Direct Observation of Oxygen Atoms in Rutile Titanium Dioxide by Spherical Aberration Corrected High-Resolution Transmission Electron Microscopy. *Nanotechnology* **2006**, *17*, 3944–3950.
22. Akita, T.; Tanaka, K.; Kohyama, M. TEM and HAADF-STEM Study of the Structure of Au Nano-Particles on CeO_2. *J. Mater. Sci.* **2008**, *43*, 3917–3922.
23. Akita, T.; Tanaka, S.; Tanaka, K.; Haruta, M.; Kohyama, M. Sequential HAADF-STEM Observation of Structural Changes in Au Nanoparticles Supported on CeO_2. *J. Mater. Sci.* **2011**, *46*, 4384–4391.
24. Yeste, M. P.; Hernandez, J. C.; Bernal, S.; Blanco, G.; Calvino, J. J.; Perez-Omil, J. A.; Pintado, J. M. Redox Behavior of Thermally Aged Ceria-Zirconia Mixed Oxides. Role of their Surface and Bulk Structural Properties. *Chem. Mater.* **2006**, *18*, 2750–2757.
25. Hernandez, J. C.; Hungria, A. B.; Perez-Omil, J. A.; Trasobares, S.; Bernal, S.; Midgley, P. A.; Alavi, A.; Calvino, J. J. Structural

Surface Investigations of Cerium-Circonium Mixed Oxide Nanocrystals with Enhanced Reducibility. *J. Phys. Chem. C* **2007**, *111*, 9001–9004.
26. Yeste, M. P.; Hernandez, J. C.; Trasobares, S.; Bernal, S.; Blanco, G.; Calvino, J. J.; Perez-Omil, J. A.; Pintado, J. M. First Stage of Thermal Aging Under Oxidizing Conditions of a $Ce_{0.62}Zr_{0.38}O_2$ Mixed Oxide with an Ordered Cationic Sublattice: A Chemical, Nanostructural, and Nanoanalytical Study. *Chem. Mater.* **2008**, *20*, 5107–5113.
27. Yeste, M. P.; Hernandez, J. C.; Bernal, S.; Blanco, G.; Calvino, J. J.; Perez-Omil, J. A.; Pintado, J. M. Comparative Study of the Reducibility Under H-2 and CO of Two Thermally Aged $Ce_{0.62}Zr_{0.38}O_2$ Mixed Oxide Samples. *Catal. Today* **2009**, *141*, 409–414.
28. Shannon, R. D. Revised Effective Ionic-Radii and Systematic Studies of Interatomic Distances in Halides and Chalcogenides. *Acta Crystallogr., Sect. A* **1976**, *32*, 751–767.
29. Williams, D. B.; Carter, C. B. *Transmission Electron Microscopy. A Textbook for Materials Science*, 2nd ed.; Plenum Press: New York, 2009; Vol. 4.
30. Moreira, P. A. F. P.; Devanathan, R.; Yu, J.; Weber, W. J. Molecular-Dynamics Simulation of Threshold Displacement Energies in Zircon. *Nucl. Instrum. Methods Phys. Res., Sect. B* **2009**, *267*, 3431–3436.
31. Garvie, L. A. J.; Buseck, P. R. Determination of Ce^{4+}/Ce^{3+} in Electron-Beam-Damaged CeO_2 by Electron Energy-Loss Spectroscopy. *J. Phys. Chem. Solids* **1999**, *60*, 1943–1947.
32. Tence, M.; Quartuccio, M.; Colliex, C. PEELS Compositional Profiling and Mapping at Nanometer Spatial-Resolution. *Ultramicroscopy* **1995**, *58*, 42–54.
33. Arenal, R.; de la Pena, F.; Stephan, O.; Walls, M.; Tence, M.; Loiseau, A.; Colliex, C. Extending the Analysis of EELS Spectrum-Imaging Data, from Elemental to Bond Mapping in Complex Nanostructures. *Ultramicroscopy* **2008**, *109*, 32–38.
34. Green, I. X.; Tang, W.; Neurock, M.; Yates, J. T., Jr. Spectroscopic Observation of Dual Catalytic Sites during Oxidation of CO on a Au/TiO_2 Catalyst. *Science* **2011**, *333*, 736–739.
35. Collins, S. E.; Cies, J. M.; del Rio, E.; Lopez-Haro, M.; Trasobares, S.; Calvino, J. J.; Pintado, J. M.; Bernal, S. Hydrogen Interaction with a Ceria-Zirconia Supported Gold Catalyst. Influence of CO Co-adsorption and Pretreatment Conditions. *J. Phys. Chem. C* **2007**, *111*, 14371–14379.
36. Gai, P. L.; Boyes, E. D. Advances in Atomic Resolution *In Situ* Environmental Transmission Electron Microscopy and 1 Angstrom Aberration Corrected *In Situ* Electron Microscopy. *Microsc. Res. Tech.* **2009**, *72*, 153–164.
37. Bernal, S.; Botana, F. J.; Calvino, J. J.; Lopez-Cartes, C.; Perez-Omil, J. A.; Rodriguez-Izquierdo, J. M. The Interpretation of HREM Images of Supported Metal Catalysts Using Image Simulation: Profile View Images. *Ultramicroscopy* **1998**, *72*, 135–164.
38. Kirkland, E. J. *Advanced Computing in Electrons Microscopy*, 2nd. ed.; Springer: New York, 2010.